

Article

Self-Cleaning Photocatalytic Polyurethane Coatings Containing Modified C₆₀ Fullerene Additives

Jeffrey G. Lundin, Spencer L. Giles, Robert F. Cozzens and James H. Wynne *

Chemistry Division, Naval Research Laboratory, 4555 Overlook Avenue SW, Washington, DC 20375, USA; E-Mails: jeffrey.lundin@nrl.navy.mil (J.G.L.); spencer.giles@nrl.navy.mil (S.L.G.); robert.cozzens@nrl.navy.mil (R.F.C.)

* Author to whom correspondence should be addressed; E-Mail: james.wynne@nrl.navy.mil; Tel.: +1-202-404-4010.

Received: 30 May 2014; in revised form: 8 July 2014 / Accepted: 25 July 2014 /

Published: 13 August 2014

Abstract: Surfaces are often coated with paint for improved aesthetics and protection; however, additional functionalities that impart continuous self-decontaminating and self-cleaning properties would be extremely advantageous. In this report, photochemical additives based on C₆₀ fullerene were incorporated into polyurethane coatings to investigate their coating compatibility and ability to impart chemical decontaminating capability to the coating surface. C₆₀ exhibits unique photophysical properties, including the capability to generate singlet oxygen upon exposure to visible light; however, C₆₀ fullerene exhibits poor solubility in solvents commonly employed in coating applications. A modified C₆₀ containing a hydrophilic moiety was synthesized to improve polyurethane compatibility and facilitate segregation to the polymer–air interface. Bulk properties of the polyurethane films were analyzed to investigate additive–coating compatibility. Coatings containing photoactive additives were subjected to self-decontamination challenges against representative chemical contaminants and the effects of additive loading concentration, light exposure, and time on chemical decontamination are reported. Covalent attachment of an ethylene glycol tail to C₆₀ improved its solubility and dispersion in a hydrophobic polyurethane matrix. Decomposition products resulting from oxidation were observed in addition to a direct correlation between additive loading concentration and decomposition of surface-residing contaminants. The degradation pathways deduced from contaminant challenge byproduct analyses are detailed.

Keywords: self-decontamination; fullerene; simulant; CWA; self-cleaning

1. Introduction

Chemical toxicants such as pesticides and toxic industrial chemicals have the potential to contaminate material surfaces for extended periods of time. Often the natural attenuation of toxic substances through evaporation and degradation in ambient environments occurs slowly due to low vapor pressure, poor solubility, and resistance to hydrolysis [1]. Due to this persistence, surfaces on which toxic chemicals reside pose human exposure risks that require application of decontamination solutions to completely render a surface safe. However, decontamination solutions and procedures are cumbersome, expensive, and often damaging to the contaminated substrate [2].

Polymeric coatings are typically applied to many surfaces to improve aesthetics and provide corrosion or weathering protection; therefore, they provide an ideal substrate to incorporate coating additives to impart continuous self-decontaminating behavior at the surface and reduce subsequent contamination. A minimal loading concentration of additive is ideal so that the properties beneficial for the originally intended purpose of the polymer coating are maintained. Specifically, polyurethanes are of the broadest interest owing to their properties such as chemical resistance and durability [3].

Several recent research developments have investigated the incorporation of novel reactive additives into various urethane coating formulations in attempts to create coatings that self-decontaminate. Antimicrobial coatings have been successfully created by imparting additives such as nonionic biocides [4], quaternary ammonium biocides [5,6], surface concentrating biocides [7], functionalized coatings [8,9], and antimicrobial peptides [10]. While these are successful biocidal additives, less success has been achieved in chemical decontaminating coatings. One reason is that additives for chemical decontamination are limited to only a few modes of action such as absorption, hydrolysis, and oxidation. Of these, oxidation offers the greatest potential to completely detoxify a broad spectrum of chemical contaminants [11].

C₆₀ fullerene molecules have also been observed to exhibit intriguing photochemical properties, including oxidative capabilities, which hold exciting potential for development of a self-decontaminating coating [12–15]. Upon exposure to visible light, C₆₀ fullerene is first excited to its singlet state C₆₀ (¹C₆₀), which then through intersystem crossing (ISC), forms the triplet state species of C₆₀ (³C₆₀). ³C₆₀ has a lifetime on the order of μs whereas ¹C₆₀ exhibits a lifetime of several ns [12,16–18]. This triplet state species of fullerene has the ability to convert ground state triplet oxygen (³Σ_g⁻) into singlet oxygen (¹Δ_g), a reactive oxygen species (ROS) [13,19]. The combination of a high quantum yield [13] and low rate of degradation of C₆₀ fullerene by ROS [12] make this molecule extremely attractive as a photo-active coating additive.

Extensive studies have been conducted to analyze and characterize the photosensitivity of C₆₀ in solution with varying degrees of success [16,19–24]. Various photosensitizers have been shown to exhibit antimicrobial activity when incorporated into polyurethane coating systems under specific conditions [25–27]. Similarly, antiviral systems have successfully been developed with the incorporation of fullerene as a solid-phase photosensitizer into biological fluid [28]. Recently, fullerenes modified with intercage constituents have displayed a remarkable ability to produce singlet oxygen as well as antimicrobial activity in polymeric adhesive films [29]. However, insertion of intercage constituents into fullerenes introduces additional cost and complexity that may be avoided by utilizing neat C₆₀.

Incorporation of C₆₀ fullerene into polymer matrices has been investigated for applications ranging from photovoltaics [30] to augmentation of polymer mechanical properties [31]. Covalent incorporation of C₆₀ fullerene into polymers offers controlled distribution and reduced leaching, albeit often at the sacrifice of photoactivity [32,33]. In contrast, non-covalent incorporation of C₆₀ fullerene offers simplified formulation and unaffected photophysical properties [34]. Furthermore, non-covalent incorporation of an amphiphilic fullerene species affords the potential for surface segregating photoactive additives. While synthetic modification of C₆₀ into an amphiphilic species most likely will affect the photophysical properties of C₆₀, increased concentration of a photoactive additive at the surface of a polymer due to its amphiphilic character should improve the decomposition of surface-residing chemical contaminants.

It can be assumed that when incorporated into a polymer matrix, the photoactivity of fullerene may be reduced due to a lack of molecular oxygen available to the fullerene molecule if it is encapsulated into the bulk of the polymeric coating. However, if one is able to overcome this limitation, significant activity should remain at the coating–air interface. It should then be expected that the production of ROS would result and subsequently react with any contamination that may be on the surface. Furthermore, an amphiphilic additive that automatically segregates to the polymer–air interface during a film cure would improve decontaminating efficiency. The hypothesis proposed herein is that the fullerene contained in the coating produces singlet oxygen from the atmosphere by the aforementioned mechanism and subsequently reacts with undesired contamination analytes that are present on the surface. If such analytes are hazardous, such as the case of pesticides or chemical warfare agents, then the action of the additive in the coating should reduce the hazard and subsequently present a surface free from contamination.

2. Experimental Section

2.1. Materials

All purchased chemicals were reagent grade and were used without further purification. The purchase of 2-chloroethyl phenyl sulfide was made at Sigma–Aldrich (St. Louis, MO, USA). Demeton-S was purchased from Chem Service (West Chester, PA, USA). Refined C₆₀ fullerene was purchased from MER Corporation (Tucson, AZ, USA).

2.2. Synthesis of EO₃–C₆₀

Covalent attachment of triethylene glycol monomethyl ether to C₆₀ fullerene through azide addition was performed following a previously described method [35]. Product was confirmed by ¹H NMR performed in CDCl₃ on a Bruker 300 MHz nuclear magnetic resonance spectrometer with a TMS internal standard. Characterization data is consistent with that previously reported [35].

2.3. Polymer Preparation

A commercial polyurethane resin, Tecoflex EG-100A (Lubrizol Advanced Materials, Inc., Gastonia, NC, USA), was employed to investigate behavior of additives in controlled polymer solutions. Polymer solutions were prepared (0.1 g polymer in 1 mL chloroform), to which photoactive additives, C₆₀ and

EO₃-C₆₀, were incorporated. After addition of additives, the solutions were vigorously vortexed to ensure complete mixing. After allowing for air bubbles to escape, polymer solutions were poured out into aluminum pans, loosely covered, and allowed to dry. Films with final additive concentrations of 0.25, 0.5, 1.0, 2.5, and 5.0 wt% were prepared.

2.4. Coating Characterization

Free coatings were peeled from aluminum backing and weighed prior to analysis on a TA Instruments (New Castle, DE, USA) DSC Q20 differential scanning calorimeter. Under a nitrogen flow of 50 mL/min, the DSC was first equilibrated to -70 °C. The temperature was then ramped from -70 °C to 170 °C at a rate of 20 °C/min. The procedure was repeated for a second scan with a ramp rate of 10 °C/min. Glass transition temperature (T_g) measurements were calculated based on the second scan using Universal Analysis 2000 software. The second scan was used for this value to eliminate any contamination of entrapped volatile and low molecular weight byproducts, as well as demonstrate hysteresis. Thermogravimetric analysis (TGA) was performed on a TA Instruments Q50 TGA employing heating rates of 10 °C/min under a N₂ atmosphere. A Thermo Scientific Nicolet 6700 FTIR (Thermo Scientific, Waltham, MA, USA) equipped with a diamond crystal ATR attachment was utilized for film analysis. Diffuse reflectance was utilized in the characterization of neat C₆₀ and EO₃-C₆₀. X-ray diffraction measurements were performed using a Rigaku SmartLab X-ray Diffractometer (XRD, Rigaku, Tokyo, Japan). The SmartLab XRD was equipped with a Cu anode operating at 3 kW generating Cu K α radiation. Measurements were taken with Bragg-Brentano Optics and a D/Tex Detector for 2-Theta measurements from 15 ° to 40 °.

Contact angle measurements were performed using a VCA Optima by AST Products, Inc. (Billerica, MA, USA) employing the sessile drop technique. Triple-distilled water was employed as a probe liquid, of which at least three replicate measurements were made for each sample. 3D laser confocal microscopy was performed on an Olympus LEXT 3D measuring laser microscope OLS4000. Surface roughness measurements were performed employing an 80 μ m cutoff wavelength (λ_c).

2.5. Contaminant Challenge

The prepared films were subjected to surface decontamination challenges against the chemical analytes presented in Figure 1, Demeton-S (**1**) and 2-chloroethyl phenyl sulfide (CEPS) (**2**), across a range of simulated environmental conditions. In general, a 2.0 μ L micropipette was used to apply 1.0 μ L of analyte to each sample (2 cm²) placed in a transparent Eppendorf tube. Each Eppendorf tube was then sealed and allowed to incubate for determined period of time in controlled conditions (darkness or simulated daylight). For photochemical reactions, a custom-built temperature controlled photochemical reactor equipped with five F8T5D fluorescent bulbs emitting broad spectrum visible light (Figure 2) at 10,000 lux intensity was employed, which simulates overcast daylight exposure. All contaminant challenges, including photochemical challenges, were performed at 20 °C. After which, residual analyte and degradation byproducts were extracted from polymer films with 1 mL of acetonitrile solution containing 12.1 mM tetrahydronaphthalene as an internal standard. Samples were then placed into a 1.5 mL GC auto-sample vial with PTFE septa top and analyzed immediately. In addition to simulant work being

performed in a fume hood, personal protective equipment consisting of nitrile gloves, lab coat, chemical safety goggles were employed at all times during handling of chemical simulants.

Figure 1. (1) Demeton-S; (2) S-vinyl degradation product; (3) CEPS; and (4) vinyl phenyl sulfoxide.

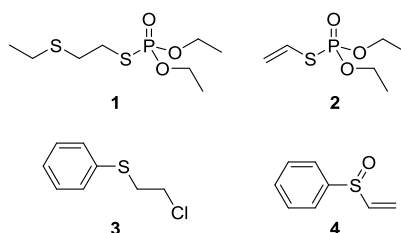
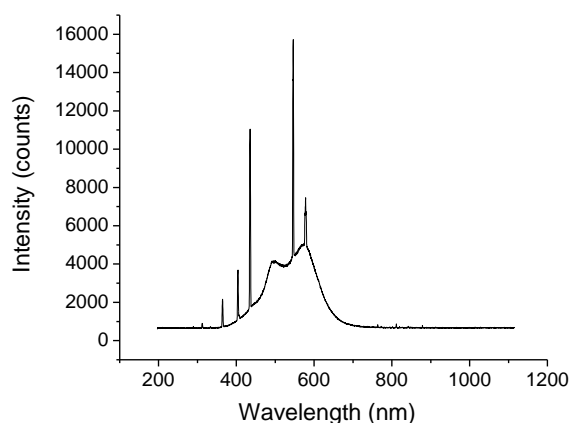


Figure 2. Emission spectrum of custom-built photochemical reactor.



Gas chromatography/mass spectroscopy (GC/MS) was employed to quantify analyte degradation. The GC/MS system consisted of an Agilent 7890A gas chromatograph equipped with an Agilent 5975C mass selective detector operating in electron ionization mode and an Agilent 7693A autoinjector. The column utilized was an Agilent HP-5MS (5% phenyl) methylpolysiloxane film. The carrier gas was helium with a flow rate of 1 mL min^{-1} . The injection volume was $1 \mu\text{L}$ with a split injection ratio of 20:1. The temperature program has an initial temperature of $100 \text{ }^\circ\text{C}$ for one minute, then $25 \text{ }^\circ\text{C per min}$ ramp to $130 \text{ }^\circ\text{C}$ followed by a $15 \text{ }^\circ\text{C per min}$ ramp to $250 \text{ }^\circ\text{C}$ with a one minute post run hold at $300 \text{ }^\circ\text{C}$. The injection temperature, MS quad temperature, and source temperature were 300 , 150 and $230 \text{ }^\circ\text{C}$, respectively. The solvent delay was set at 1.5 min and detector was set to scan a mass range of 20 to 350 m/z. Prior to comparison, GC/MS results were normalized by dividing the analyte peak area by the peak area of the internal standard, tetrahydronaphthalene.

3. Results and Discussion

3.1. Additive–Polymer Compatibility

Additive–polymer compatibility and the effects of photoactive additive incorporation on Tecoflex film properties were investigated with a variety of methods. ATR-IR analysis was performed to investigate the effect of C_{60} incorporation on infrared signature and probe the chemical composition of the polymer film. ATR-IR analysis confirmed that the low loading concentrations employed in this study

allowed the chemical signature of polymer film to be maintained despite increasing concentrations of C_{60} and EO_3-C_{60} .

Effects of additive incorporation on Tecoflex films on thermal stability were investigated with TGA. The incorporation of C_{60} and EO_3-C_{60} into Tecoflex films each resulted in an increased thermal stability (Table 1). The incorporation of EO_3-C_{60} in Tecoflex resulted in increased thermal stability (temperature at 10% loss) that scaled linearly with loading concentration. The increase in initial thermal stability suggests that stabilizing intermolecular interactions are occurring between EO_3-C_{60} and Tecoflex polymer. Generally, the incorporation of C_{60} into Tecoflex demonstrated a moderate increase in thermal stability. A weak inverse relationship was observed with increased loading of C_{60} and thermal stability, as opposed to the direct relationship of EO_3-C_{60} loading. This suggests that with increased loading concentration, additional C_{60} aggregates to other C_{60} instead of interacting with polymer matrix. Additionally, the lessened effect on thermal stability upon C_{60} incorporation compared to EO_3-C_{60} indicates that EO_3-C_{60} interacts more strongly than C_{60} with Tecoflex polymer matrix. The greater favorable interactions between EO_3-C_{60} and Tecoflex results from compatibility between the ethylene oxide tail of EO_3-C_{60} and the ether regions of the butane diol constituents of the Tecoflex monomer.

Table 1. Thermal properties of Tecoflex films.

Tecoflex Film	10% Loss (°C)	Mass Remaining (%) *
Control	300.55	0.2727
0.5% C_{60}	314.99	1.463
1.0% C_{60}	311.07	2.561
2.5% C_{60}	307.38	6.574
5.0% C_{60}	309.86	11.25
0.25% EO_3-C_{60}	312.61	0.6591
0.5% EO_3-C_{60}	319.44	0.7918
1.0% EO_3-C_{60}	325.63	1.513

* At 600 °C.

TGA analysis also indicated that incorporation of C_{60} into Tecoflex resulted in greater ultimate mass remaining than those loaded with EO_3-C_{60} . The alkoxy moiety of the EO_3-C_{60} is susceptible to thermal degradation at a greater temperature than the fullerene cage of C_{60} . Therefore, each comparable loading concentration of C_{60} (720 g/mol) and EO_3-C_{60} (881 g/mol) contains a 1.22-fold molar excess of C_{60} to EO_3-C_{60} . Thus, the thermal degradation of the alkoxy tail of EO_3-C_{60} below 600 °C results in only 82% remaining of the total loaded EO_3-C_{60} . Considering this, at 600 °C, there should be approximately a 1.5 × excess remaining mass % of C_{60} relative to EO_3-C_{60} at comparable loading concentrations. Indeed, such an excess was observed upon comparison of the 1 wt% loadings.

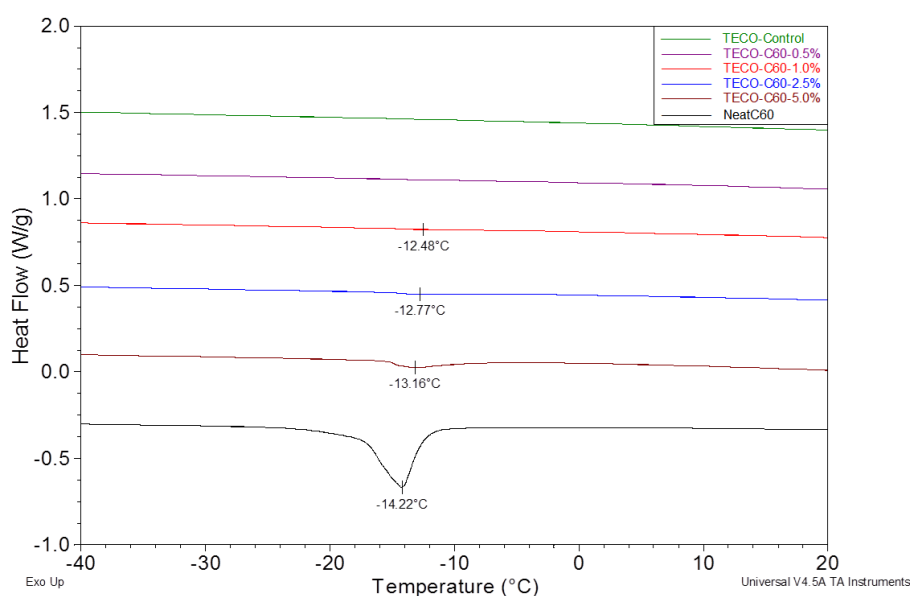
Interestingly, the ultimate wt% for each Tecoflex film containing additives was greater than the additive wt% loading concentration (Table 1). The amount of mass remaining from the thermal degradation of Tecoflex films containing C_{60} at 600 °C corresponded to approximately double the C_{60} loading concentration. This indicates one of two possibilities: a quantity of Tecoflex polymer is strongly adhered to the surface of C_{60} fullerene through intermolecular forces that require greater than 600 °C to dissociate or aggregation of C_{60} results in thermally stabilized Tecoflex polymer trapped within the aggregate. However, the lower thermal degradation onset temperature of Tecoflex films containing C_{60}

rather than $\text{EO}_3\text{-C}_{60}$ revealed that intermolecular interactions were stronger for $\text{EO}_3\text{-C}_{60}$. The difference between the final mass remaining and loading concentration decreased with increased additive loading concentration of both C_{60} and $\text{EO}_3\text{-C}_{60}$, suggesting that with increased loading concentration, additional intermolecular C_{60} aggregation occurs instead of C_{60} -polymer matrix interactions. The deviation was greater for C_{60} than it was for $\text{EO}_3\text{-C}_{60}$, indicating that aggregation is more prominent in C_{60} than $\text{EO}_3\text{-C}_{60}$.

DSC was performed on all Tecoflex films to investigate effects of additive incorporation on glass transition temperature (T_g). The way in which additive incorporation affects T_g can afford insight into intermolecular interactions between the additive and polymer. Increase in T_g resulting from additive incorporation indicates increased intermolecular interactions that limit polymer mobility [36]. Unmodified Tecoflex exhibits a glass transition that spans a broad temperature range. Incorporation of additives, both C_{60} and $\text{EO}_3\text{-C}_{60}$, result in minor and insignificant effects on T_g , thus indicating that the integrity of the coating was preserved.

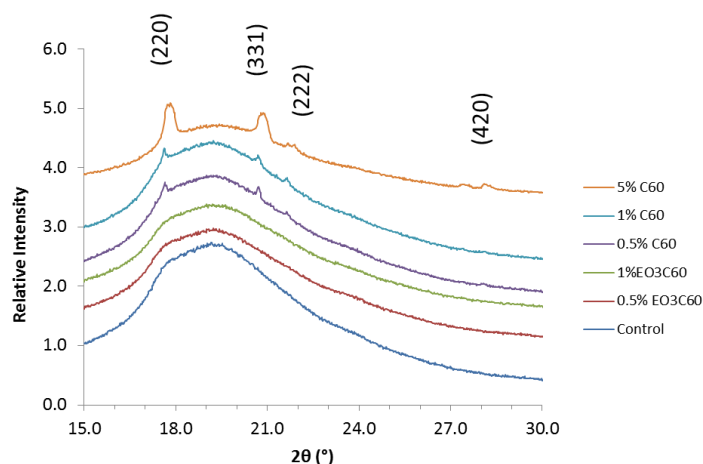
For both neat C_{60} and Tecoflex films containing higher concentrations of C_{60} , an endothermic transition was observed in the DSC thermograms at approximately -14°C . The magnitude of the endothermic peak increases corresponding to C_{60} concentration (Figure 3). This endotherm corresponds to the phase transition of C_{60} crystals from simple cubic orientation ordering to face-centered cubic structure upon heating through the transition temperature [37,38]. The presence of this transition from Tecoflex films indicates a crystalline phase of C_{60} fullerene. C_{60} can only be in a crystalline phase when multiple fullerene molecules are in contact with one another, or aggregated, in a regular, repeated order. A polymeric film in which C_{60} fullerene was completely dispersed would not exhibit such crystalline phase transition. Furthermore, endotherm corresponding to the simple cubic to face-centered cubic phase transition was absent in the DSC analysis of neat $\text{EO}_3\text{-C}_{60}$ and the Tecoflex films containing $\text{EO}_3\text{-C}_{60}$. Therefore, aggregation, or at least the formation of crystallites, of C_{60} is inhibited by the covalent modification of C_{60} with ethylene oxide tails. Furthermore, the amphiphilic character of the $\text{EO}_3\text{-C}_{60}$ improves solubility of the additive in the Tecoflex solution and facilitates increased molecular dispersion of the additive throughout the polymer matrix.

Figure 3. Comparison of DSC thermograms for Tecoflex films containing C_{60} and neat C_{60} .



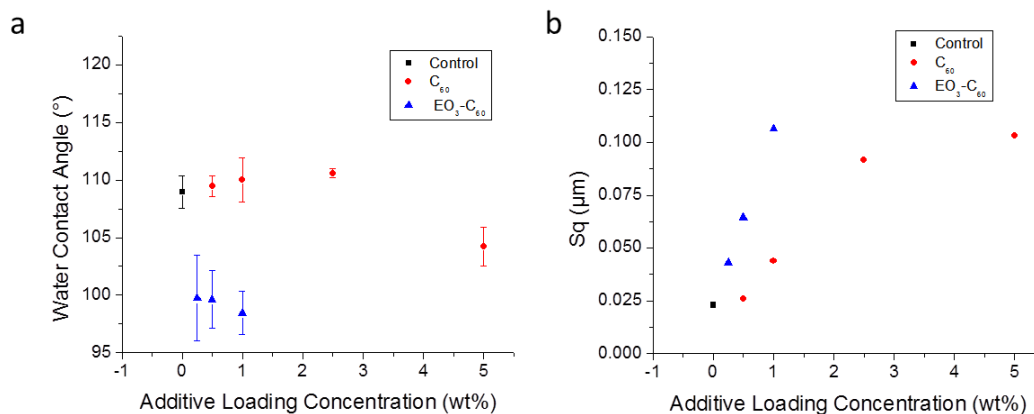
X-ray diffraction analysis (Figure 4) confirmed crystallinity observed via DSC. Diffraction peaks corresponding to the (220), (331), (222), and (420) peaks of crystallized C_{60} were observed in the Tecoflex films containing unmodified C_{60} additive. The intensity of diffraction peaks increased with increased loading of C_{60} from 0.5 to 5.0 wt%. In contrast, control Tecoflex and Tecoflex loaded with EO_3-C_{60} displayed only a broad peak resulting from the amorphous polymer. Therefore, C_{60} aggregates into crystals in Tecoflex matrix, while EO_3-C_{60} is well dispersed.

Figure 4. XRD patterns of Tecoflex films containing additives.



Water contact angle measurements were performed on Tecoflex films containing C_{60} and EO_3-C_{60} , the results of which are shown in Figure 5. Addition of C_{60} in Tecoflex resulted in minor increases in water contact angle in loadings up to 2.5 wt% and ultimately a minor decrease at 5 wt% C_{60} loading. Correspondingly, the surface roughness of Tecoflex films increased with increased C_{60} loading. On the other hand, loading of EO_3-C_{60} in Tecoflex resulted in a significant decrease in water contact angle accompanied with a linear increase surface roughness to a greater degree than C_{60} . Therefore, comparison of contact angle and surface roughness indicates that surface roughness plays an insignificant role in the water contact angle, despite previous evidence to the contrary [39]. Thus the affect that additive loading has on water contact angle must result from the additive's effect on the surface energy of Tecoflex, instead of imparted surface roughness.

Figure 5. Water contact angle (a) and surface roughness (b), S_q , of Tecoflex films loaded with C_{60} and EO_3-C_{60} .



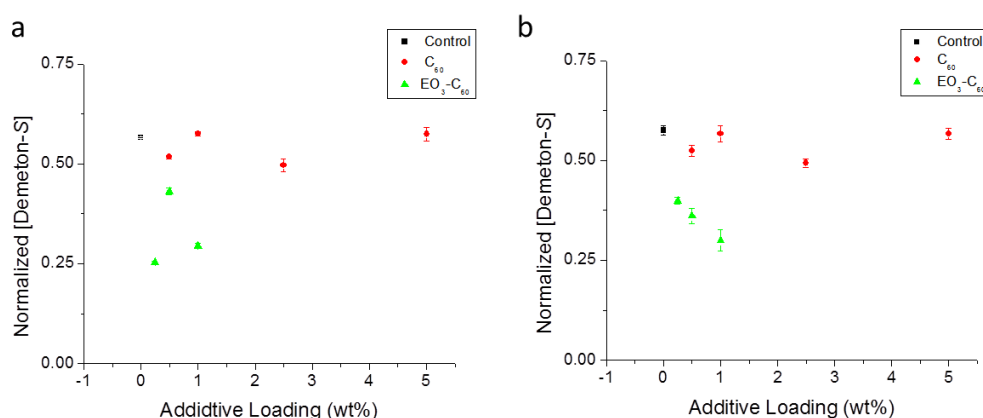
The covalent attachment of ethylene glycol moiety to C_{60} results in a molecule with amphiphilic character, *i.e.*, a surfactant. When incorporated into a solution of hydrophobic Tecoflex, the amphiphilic EO_3-C_{60} has the potential to orient its hydrophilic moiety at the polymer–air interface in order to minimize solvophobic interactions between hydrophilic ethylene oxide and hydrophobic Tecoflex matrix. Indeed, a linear decrease in contact angle was observed between 0.25 and 1.0 wt% loadings of EO_3-C_{60} . Considering that the highest loading (5%) of C_{60} in Tecoflex resulted in decrease in water contact angle of only 4° , the significant decrease in water contact angle (increase in hydrophilicity) of 10° at only 1 wt% loading of EO_3-C_{60} indicates that the additive is concentrated at the surface of the polyurethane film.

3.2. Decontamination Challenges

Decontamination challenges were employed to investigate the capability imparted by photoactive additives C_{60} and EO_3-C_{60} onto Tecoflex films to automatically decompose surface-residing contaminants. Two chemical compounds, Demeton-*S* and CEPS, were employed as representative contaminants of organophosphorous and sulfide-based pesticides. The prepared films were first subjected to decontamination challenges consisting of 18 h contaminant residence time.

Figure 6 presents results from a 4 g/m^2 Demeton-*S* decontamination challenge in which extracted Demeton-*S* (normalized by the tetralin internal standard) is plotted against additive loading concentration. No correlation was observed between C_{60} loading concentration in Tecoflex films and Demeton-*S* reduction. Furthermore, reduction of Demeton-*S* on C_{60} exhibits similar trends in both dark and light conditions. Tecoflex films containing EO_3-C_{60} exhibit increased reduction of Demeton-*S* compared to films containing C_{60} in dark conditions; however, decomposition of Demeton-*S* did not directly correlate with additive loading. Tecoflex films exposed to light that contained EO_3-C_{60} exhibit direct correlation between reduction of Demeton-*S* and EO_3-C_{60} loading concentration. From this, it is proposed that different modes of action for Demeton-*S* degradation are occurring between Tecoflex films containing C_{60} and EO_3-C_{60} , thus necessitating decomposition byproducts analysis.

Figure 6. Demeton-*S* recovered from Tecoflex films after 18 h residence in dark (a) and daylight (b) conditions.



Byproduct analysis of the 18 h Demeton-*S* decontamination challenges were performed for further insight into possible modes of action. In addition to reduction in Demeton-*S*, significant byproducts were

detected at a retention time of 4.1 min which corresponds to vinyl oxidation product (*S*-vinyl) (**2**). Byproduct concentration, normalized with the internal standard, is plotted against loading concentration in Figure 7. It is apparent that increased C₆₀ loading leads to decreased production of **2** in both dark and light conditions, whereas increasing concentration of EO₃-C₆₀ loading results in increasing production of **2**. Unmodified C₆₀ is more reactive than EO₃-C₆₀, especially at low concentrations; however, increased concentration of C₆₀ does not result in increased decomposition, most likely due to self-quenching resulting from high C₆₀ proximity from aggregation in the polymer matrix. Qualitative observation indicated that poor solubility of C₆₀ in chloroform facilitates the formation of C₆₀ aggregates, in which the probability of self-quenching between C₆₀ molecules is increased.

For Tecoflex films containing C₆₀, comparable amounts of **2** were detected from decomposition of Demeton-*S* on films that resided in dark and light conditions for 18 h (Figure 7a). From this, it appears that photoactivity against Demeton-*S* is not occurring in the Tecoflex films containing unmodified C₆₀. If photoactivity was occurring, then a greater amount of **2** would be observed on the films exposed to light than in darkness. It has been previously demonstrated that C₆₀ fullerene can behave as an electron acceptor (Lewis acid) toward sulfides [40]. Thus, the electron acceptor behavior of C₆₀ in Tecoflex may facilitate the cleavage of the S-C bond (Figure 8) resulting in the elimination product **2**.

Figure 7. Detected *S*-vinyl product (shown as normalized ratio of *S*-vinyl peak area to tetralin peak area) from Tecoflex films loaded with C₆₀ (a) and EO₃-C₆₀ (b) over an 18 h Demeton-*S* challenge.

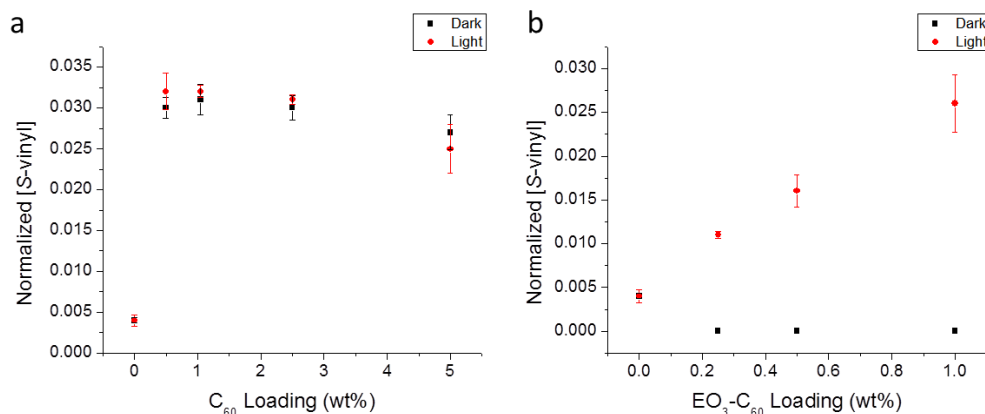
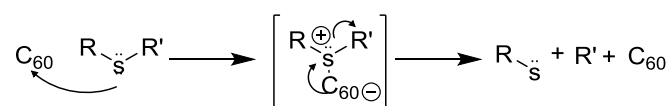


Figure 8. Hypothesized Lewis acid catalyzed sulfide elimination.

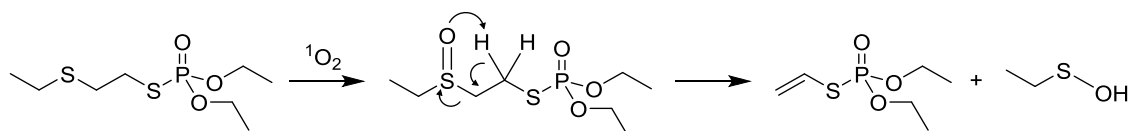


On the other hand, photoactivity was apparent from byproduct analysis in the films loaded with EO₃-C₆₀ (Figure 7b). In fact, the photoactivity of EO₃-C₆₀ continued to increase with increasing concentration indicating that the ethylene oxide moieties, by improving solubility, help to diminish aggregate facilitated self-quenching. In contrast to the films containing C₆₀, an absence of Demeton-*S* decomposition on Tecoflex films containing EO₃-C₆₀ in dark conditions was observed. This is likely the result of decreased Lewis acid character upon the covalent attachment of the ethylene oxide moiety.

The combination of photoactivity and oxidation products detected from Tecoflex films containing $\text{EO}_3\text{-C}_{60}$, and documented capability of fullerene species to photogenerate singlet oxygen [41] has led to the proposed mode of action for Demeton-*S* decomposition on films containing $\text{EO}_3\text{-C}_{60}$ exposed to visible light presented in Figure 9. The photoactive species embedded in the polymer matrix is first photosensitized upon the absorption of visible light. Subsequent transfer of energy from photosensitized $\text{EO}_3\text{-C}_{60}$ to ambient atmospheric oxygen results in the formation of singlet oxygen ($^1\text{O}_2$). The photogenerated singlet oxygen, a ROS, then oxidizes the peripheral sulfur of Demeton-*S* that is residing on the coating surface in proximity to the photosensitized additive. The sulfoxide then undergoes α elimination resulting in the Demeton-*S* vinyl degradation product (**2**) and unstable sulfenic acid, which quickly self-condenses to form the corresponding thiosulfanate.

In addition to decontamination challenges against Demeton-*S*, Tecoflex films loaded with photoactives were also subjected to CEPS decontamination challenges. An 18 h decontamination challenge was initially performed for each sample in both dark and light conditions. Despite minor differences in the amount of CEPS decomposed, significant differences in byproduct formation were observed to be dependent on the conditions in which the sample resided.

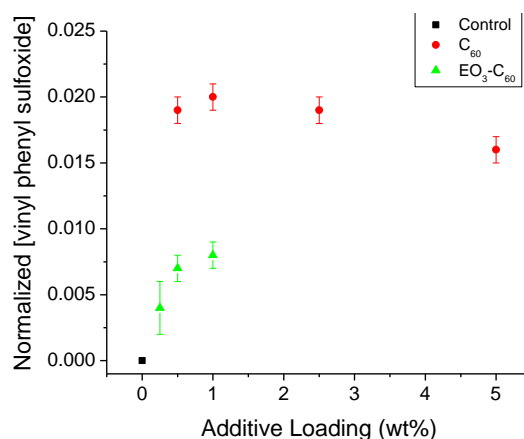
Figure 9. Proposed oxidation mechanism of Demeton-*S* and the formation of elimination product from photogenerated singlet oxygen.



GC-MS analysis afforded the detection of a notable degradation product of CEPS from the Tecoflex films containing photoactives that resided in daylight conditions. Mass spectra analysis determined that the degradation product was vinyl phenyl sulfoxide (**4**), an oxidation byproduct of CEPS (Figure 1). Furthermore, **4** was not detected from coatings that resided in dark conditions. Figure 10 presents normalized concentrations of **4** detected in the reaction extract from Tecoflex films loaded with C_{60} and $\text{EO}_3\text{-C}_{60}$ after an 18 h residence time of CEPS. Production of **4** from Tecoflex films decreases with increasing C_{60} loading concentration. This is attributed to increasing C_{60} aggregation with increased C_{60} loading concentration due to poor solubility and incompatibility with the polyurethane matrix, as previously demonstrated via DSC and XRD. The increase in aggregation effectively limits the available surface area of C_{60} available for both singlet oxygen generation and contact with the contaminant. Additionally, singlet oxygen quenching is known to occur between proximal C_{60} molecules in high concentration, such as in aggregates and crystallites [42].

In contrast to the effects observed resulting from C_{60} loading concentration, the generation of **4** increased with increasing $\text{EO}_3\text{-C}_{60}$ concentration in Tecoflex from 0.25 to 1.0 wt%. This direct correlation of $\text{EO}_3\text{-C}_{60}$ loading and generation of **4** can only result from minimized self-quenching due to good dispersion of $\text{EO}_3\text{-C}_{60}$. These trends support those that were observed in the Demeton-*S* decontamination challenge.

Figure 10. CEPS byproduct resulting from residence on Tecoflex films of several additive concentrations following exposure to daylight conditions for 18 h.



From the above 18 h study, 1 wt% loadings of C₆₀ and EO₃-C₆₀ were down-selected for an expanded time-dependent CEPS decontamination challenge over the course of 165 h in daylight conditions (Figure 11). Figure 11a displays concentration of CEPS extracted from samples over a 165 h residence time period. Each of the films subjected to the challenge exhibited rapid decrease in CEPS concentration over the first 48 h. This is attributed to inherent attenuation of CEPS as this behavior was observed on the two controls, a Teflon film and unmodified Tecoflex. C₆₀ and EO₃-C₆₀ films differentiate from the controls at time points beyond 48 h, after which the degradation rates of CEPS on the controls decrease drastically. In contrast, the C₆₀ and EO₃-C₆₀ Tecoflex films exhibit continued linear degradation of CEPS beyond 48 h. This behavior is explained by two separate degradation mechanisms occurring simultaneously. First, the attenuation mechanism, which is initially at a high rate, dominates the first 48 h of degradation. Beyond 48 h, attenuation rate slows to an extent such that the secondary mechanism, photo-oxidation, dominates the overall reaction rate and thus becomes apparent.

Byproduct analysis (Figure 11b) confirms linear increase of oxidation product (4) over time on films containing photoactive additives. Tecoflex films containing C₆₀ and EO₃-C₆₀ each exhibited a linear relationship between production of oxidation product and residence time, while oxidation was not detected from the controls. The detection of oxidation products only from samples that are exposed to light, that contain either C₆₀ or EO₃-C₆₀, and dependent on the concentration of C₆₀ and EO₃-C₆₀ indicates that a photo-mediated oxidation process is facilitating the oxidation of CEPS.

In consideration of the data presented herein and the known singlet oxygen generation potential of C₆₀ fullerene, a proposed mode of action for CEPS oxidation is presented in Figure 12. Similar to the mechanism proposed for the oxidation of Demeton-S, the photoactive in Tecoflex generates singlet oxygen upon exposure to light. Singlet oxygen oxidizes the S atom to sulfoxide, which then through an elimination mechanism produces a vinyl sulfoxide with HCl as a byproduct. In contrast to the mechanism proposed for Demeton-S, the oxygen remains on the same byproduct molecule as sulfur. This is due to the stability of the sulfenic acid leaving group in Demeton-S decomposition compared to the instability of the potential hypochlorite byproduct in CEPS oxidation.

Figure 11. Concentration of CEPS recovered from samples over a 165 h residence (a) and normalized vinyl phenyl sulfoxide degradation product (b).

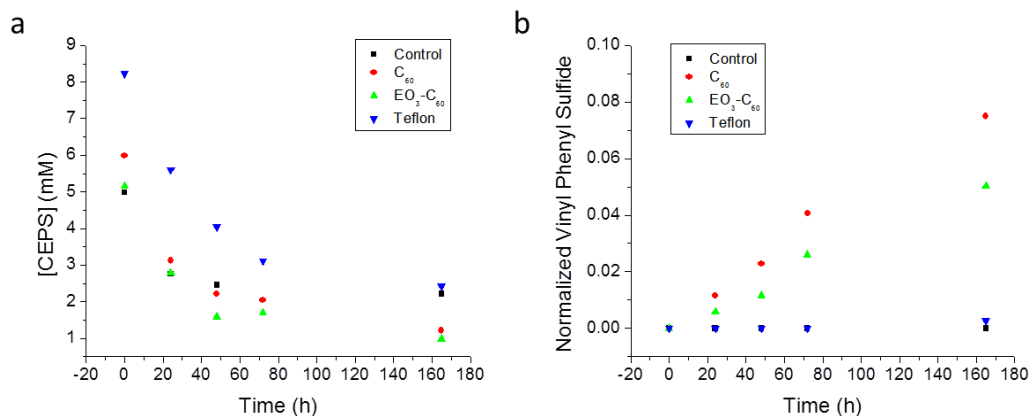
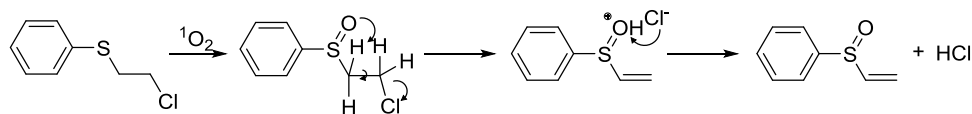


Figure 12. Potential pathway of sulfide oxidation followed by dehydrohalogenation of CEPS.



4. Conclusions

Several insights were gained upon the incorporation of C₆₀ and EO₃-C₆₀ into Tecoflex films. The detection of the phase transition from simple cubic to face-centered cubic structure at approximately -14 °C, subsequent confirmation with XRD, and the decreased reactivity against simulants at increased C₆₀ loading concentrations provide evidence of C₆₀ aggregation in Tecoflex films. Conversely, no such evidence was observed to indicate that EO₃-C₆₀ was aggregating in Tecoflex films. Therefore, the covalent attachment of ethylene glycol tail to C₆₀ results in an additive that exhibits improved solubility and dispersion in the hydrophobic polyurethane matrix of Tecoflex.

Surface decontamination challenges demonstrated the self-cleaning capability of Tecoflex films containing C₆₀ and EO₃-C₆₀ additives. Decomposition products resulting from oxidation were observed in addition to a direct correlation between additive loading concentration and decomposition of surface-residing contaminants. Through correlation of trends observed from Demeton-S and CEPS decontamination challenges and byproduct analysis, modes of action were proposed for the decomposition pathways of both contaminants on the surface of polyurethane films.

Acknowledgments

This work was funded by the Office of Naval Research (ONR) and the Naval Research Laboratory.

Author Contributions

Jeffrey G. Lundin prepared polymer films, acquired and analyzed various data, and composed the manuscript. Spencer L. Giles performed XRD data acquisition and analysis. Robert F. Cozzens assisted

in interpretation of degradation reactions. James H. Wynne assisted in manuscript revision and project management.

Conflicts of Interest

The authors declare no conflict of interest.

References

1. Bartelt-Hunt, S.L.; Knappe, D.R.U.; Barlaz, M.A. A review of chemical warfare agent simulants for the study of environmental behavior. *Crit. Rev. Environ. Sci. Technol.* **2008**, *38*, 112–136.
2. Gephart, R.T.; Coneski, P.N.; Wynne, J.H. Decontamination of chemical-warfare agent simulants by polymer surfaces doped with the singlet oxygen generator zinc octaphenoxypthalocyanine. *ACS Appl. Mater. Interfaces* **2013**, *5*, 10191–10200.
3. Chattopadhyay, D.K.; Raju, K.V.S.N. Structural engineering of polyurethane coatings for high performance applications. *Prog. Polym. Sci.* **2007**, *32*, 352–418.
4. Wynne, J.H.; Pant, R.R.; Jones-Meehan, J.M.; Phillips, J.P. Preparation and evaluation of nonionic amphiphilic phenolic biocides in urethane hydrogels. *J. Appl. Polym. Sci.* **2008**, *107*, 2089–2094.
5. Pant, R.R.; Buckley, J.L.; Fulmer, P.A.; Wynne, J.H.; McCluskey, D.M.; Phillips, J.P. Hybrid siloxane epoxy coatings containing quaternary ammonium moieties. *J. Appl. Polym. Sci.* **2008**, *110*, 3080–3086.
6. Kurt, P.; Wood, L.; Ohman, D.E.; Wynne, K.J. Highly effective contact antimicrobial surfaces via polymer surface modifiers. *Langmuir* **2007**, *23*, 4719–4723.
7. Harney, M.B.; Pant, R.R.; Fulmer, P.A.; Wynne, J.H. Surface self-concentrating amphiphilic quaternary ammonium biocides as coating additives. *ACS Appl. Mater. Interfaces* **2009**, *1*, 39–41.
8. Pant, R.R.; Fulmer, P.A.; Harney, M.B.; Buckley, J.P.; Wynne, J.H. Synthesis and biocidal efficacy of self-spreading polydimethylsiloxane oligomers possessing oxyethylene-functionalized quaternary ammoniums. *J. Appl. Polym. Sci.* **2009**, *113*, 2397–2403.
9. Pant, R.R.; Rasley, B.T.; Buckley, J.P.; Lloyd, C.T.; Cozzens, R.F.; Santangelo, P.G.; Wynne, J.H. Synthesis, mobility study and antimicrobial evaluation of novel self-spreading ionic silicone oligomers. *J. Appl. Polym. Sci.* **2007**, *104*, 2954–2964.
10. Fulmer, P.A.; Lundin, J.G.; Wynne, J.H. Development of antimicrobial peptides (amps) for use in self-decontaminating coatings. *ACS Appl. Mater. Interfaces* **2010**, *2*, 1266–1270.
11. Talmage, S.S.; Watson, A.P.; Hauschild, V.; Munro, N.B.; King, J. Chemical warfare agent degradation and decontamination. *Curr. Org. Chem.* **2007**, *11*, 285–298.
12. Arbogast, J.W.; Darmanyan, A.P.; Foote, C.S.; Diederich, F.N.; Whetten, R.L.; Rubin, Y.; Alvarez, M.M.; Anz, S.J. Photophysical properties of sixty atom carbon molecule (C₆₀). *J. Phys. Chem.* **1991**, *95*, 11–12.
13. Nagano, T.; Arakane, K.; Ryu, A.; Masunaga, T.; Shinmoto, K.; Mashiko, S.; Hirobe, M. Comparison of singlet oxygen production efficiency of C₆₀ with other photosensitizers, based on 1268 nm emission. *Chem. Pharm. Bull.* **1994**, *42*, 2291–2294.

14. Pichler, K.; Graham, S.; Gelsen, O.M.; Friend, R.H.; Romanow, W.J.; McCauley, J.P., Jr.; Coustel, N.; Fischer, J.E.; Smith, A.B. Photophysical properties of solid films of fullerene, C₆₀. *J. Phys. Condens. Matter* **1991**, *3*, 9259–9270.
15. Wasielewski, M.R.; O’Neil, M.P.; Lykke, K.R.; Pellin, M.J.; Gruen, D.M. Triplet states of fullerenes C₆₀ and C₇₀. Electron paramagnetic resonance spectra, photophysics, and electronic structures. *J. Am. Chem. Soc.* **1991**, *113*, 2774–2776.
16. Hotze, E.M.; Labille, J.; Alvarez, P.; Wiesner, M.R. Mechanisms of photochemistry and reactive oxygen production by fullerene suspensions in water. *Environ. Sci. Technol.* **2008**, *42*, 4175–4180.
17. Haufler, R.E.; Wang, L.-S.; Chibante, L.P.F.; Jin, C.; Conceicao, J.; Chai, Y.; Smalley, R.E. Fullerene triplet state production and decay: R2PI probes of C₆₀ and C₇₀ in a supersonic beam. *Chem. Phys. Lett.* **1991**, *179*, 449–454.
18. Fraelich, M.R.; Weisman, R.B. Triplet states of fullerene C₆₀ and C₇₀ in solution: Long intrinsic lifetimes and energy pooling. *J. Phys. Chem.* **1993**, *97*, 11145–11147.
19. Orfanopoulos, M.; Kambourakis, S. Chemical evidence of singlet oxygen production from C₆₀ and C₇₀ in aqueous and other polar media. *Tetrahedron Lett.* **1995**, *36*, 435–438.
20. Lee, J.; Fortner, J.D.; Hughes, J.B.; Kim, J.-H. Photochemical production of reactive oxygen species by C₆₀ in the aqueous phase during uv irradiation. *Environ. Sci. Technol.* **2007**, *41*, 2529–2535.
21. Lee, J.; Mackeyev, Y.; Cho, M.; Li, D.; Kim, J.-H.; Wilson, L.J.; Alvarez, P.J.J. Photochemical and antimicrobial properties of novel C₆₀ derivatives in aqueous systems. *Environ. Sci. Technol.* **2009**, *43*, 6604–6610.
22. Lee, J.; Yamakoshi, Y.; Hughes, J.B.; Kim, J.-H. Mechanism of C₆₀ photoreactivity in water: Fate of triplet state and radical anion and production of reactive oxygen species. *Environ. Sci. Technol.* **2008**, *42*, 3459–3464.
23. Deguchi, S.; Alargova, R.G.; Tsujii, K. Stable dispersions of fullerenes, C₆₀ and C₇₀, in water. Preparation and characterization. *Langmuir* **2001**, *17*, 6013–6017.
24. Lyon, D.Y.; Adams, L.K.; Falkner, J.C.; Alvarez, P.J.J. Antibacterial activity of fullerene water suspensions: Effects of preparation method and particle size. *Environ. Sci. Technol.* **2006**, *40*, 4360–4366.
25. Wilson, M. Light-activated antimicrobial coating for the continuous disinfection of surfaces. *Infect. Control Hosp. Epidemiol.* **2003**, *24*, 782–784.
26. Page, K.; Wilson, M.; Parkin, I.P. Antimicrobial surfaces and their potential in reducing the role of the inanimate environment in the incidence of hospital-acquired infections. *J. Mater. Chem.* **2009**, *19*, 3818–3831.
27. Perni, S.; Piccirillo, C.; Pratten, J.; Prokopovich, P.; Chrzanowski, W.; Parkin, I.P.; Wilson, M. The antimicrobial properties of light-activated polymers containing methylene blue and gold nanoparticles. *Biomaterials* **2009**, *30*, 89–93.
28. Belousova, I.M.; Danilov, O.B.; Muraveva, T.D.; Kiselyakov, I.M.; Rylkov, V.V.; Krisko, T.K.; Kiselev, O.I.; ZarubaeV, V.V.; Sirotkin, A.K.; Piotrovskii, L.B. Solid-phase photosensitizers based on fullerene C₆₀ for photodynamic inactivation of viruses in biological liquids. *J. Opt. Technol.* **2009**, *76*, 243–250.

29. McCluskey, D.M.; Smith, T.N.; Madasu, P.K.; Coumbe, C.E.; Mackey, M.A.; Fulmer, P.A.; Wynne, J.H.; Stevenson, S.; Phillips, J.P. Evidence for singlet-oxygen generation and biocidal activity in photoresponsive metallic nitride fullerene-polymer adhesive films. *ACS Appl. Mater. Interfaces* **2009**, *1*, 882–887.
30. Vandewal, K.; Albrecht, S.; Hoke, E.T.; Graham, K.R.; Widmer, J.; Douglas, J.D.; Schubert, M.; Mateker, W.R.; Bloking, J.T.; Burkhard, G.F.; *et al.* Efficient charge generation by relaxed charge-transfer states at organic interfaces. *Nat. Mater.* **2014**, *13*, 63–68.
31. Badamshina, E.; Estrin, Y.; Gafurova, M. Nanocomposites based on polyurethanes and carbon nanoparticles: Preparation, properties and application. *J. Mater. Chem. A* **2013**, *1*, 6509–6529.
32. Giacalone, F.; Mart ń, N. Fullerene polymers: Synthesis and properties. *Chem. Rev.* **2006**, *106*, 5136–5190.
33. Accorsi, G.; Armaroli, N. Taking advantage of the electronic excited states of [60]-fullerenes. *J. Phys. Chem. C* **2010**, *114*, 1385–1403.
34. Badamshina, E.; Gafurova, M. Polymeric nanocomposites containing non-covalently bonded fullerene C₆₀: Properties and applications. *J. Mater. Chem.* **2012**, *22*, 9427–9438.
35. Hawker, C.J.; Saville, P.M.; White, J.W. The synthesis and characterization of a self-assembling amphiphilic fullerene. *J. Org. Chem.* **1994**, *59*, 3503–3505.
36. Teh, S.-L.; Linton, D.; Sumpter, B.; Dadmun, M.D. Controlling non-covalent interactions to modulate the dispersion of fullerenes in polymer nanocomposites. *Macromolecules* **2011**, *44*, 7737–7745.
37. Sachidanandam, R.; Harris, A.B. Comment on “orientational ordering transition in solid C₆₀”. *Phys. Rev. Lett.* **1991**, *67*, 1467–1467.
38. Heiney, P.A.; Fischer, J.E.; McGhie, A.R.; Romanow, W.J.; Denenstein, A.M.; McCauley, J.P., Jr.; Smith, A.B.; Cox, D.E. Orientational ordering transition in solid C₆₀. *Phys. Rev. Lett.* **1991**, *66*, 2911–2914.
39. Bellanger, H.; Darmanin, T.; Taffin de Givenchy, E.; Guittard, F. Chemical and physical pathways for the preparation of superoleophobic surfaces and related wetting theories. *Chem. Rev.* **2014**, *114*, 2694–2716.
40. Zhang, J.Z.; Geselbracht, M.J.; Ellis, A.B. Binding of fullerenes to cadmium sulfide and cadmium selenide surfaces, photoluminescence as a probe of strong, lewis acidity-driven, surface adduct formation. *J. Am. Chem. Soc.* **1993**, *115*, 7789–7793.
41. Phillips, J.P.; Deng, X.; Todd, M.L.; Heaps, D.T.; Stevenson, S.; Zhou, H.; Hoyle, C.E. Singlet oxygen generation and adhesive loss in stimuli-responsive, fullerene-polymer blends, containing polystyrene-block-polybutadiene-block-polystyrene and polystyrene-block-polyisoprene-block-polystyrene rubber-based adhesives. *J. Appl. Polym. Sci.* **2008**, *109*, 2895–2904.
42. Bagrov, I.; Belousova, I.; Danilov, O.; Kiselev, V.; Murav’eva, T.; Sosnov, E. Photoinduced quenching of the luminescence of singlet oxygen in fullerene solutions. *Opt. Spectrosc.* **2007**, *102*, 52–59.